In-situ Evidence of the Redox-State Dependence of Photoluminescence in Graphene Quantum Dots

Joaquin Barrera,[a] *David Ibañez,*[a] *Aranzazu Heras,*[a] *Virginia Ruiz,*,*[b] *and Alvaro Colina*,*[a]

a. Department of Chemistry, Universidad de Burgos, Pza. Misael Bañuelos s/n, E-09001 Burgos, Spain. Fax: +34 947258831; Tel: +34 947258817;

b. IK4-CIDETEC, Materials Division, Pº Miramón 196, E-20009 San Sebastián, Spain.

Corresponding Author

* E-mail: acolina@ubu.es, vruiz@cidetec.es

ABSTRACT

Changes in the optical properties of Graphene Quantum Dots (GQD) during electrochemical reduction and oxidation were investigated by photoluminescence (PL) spectroelectrochemistry, which provided direct in-situ evidence of the dependence of GQD luminescence on their redox state. We demonstrated that GQD PL intensity was enhanced upon reduction (quantum yield increased from 0.44 to 0.55) and substantially bleached during oxidation (quantum yield ~0.12).

Moreover, PL emission blue/red shifted upon GQD reduction/oxidation, rendering information about electronic transitions involved in the redox processes, namely the $\pi \rightarrow \pi^*$ and the $n \rightarrow \pi^*$ transitions between energy levels of the aromatic sp^2 domains and the functional groups, respectively. PL intensity changes during GQD reduction/oxidation resulted from a variation in structural changes in GQD as a result of charge injection, as corroborated by in-situ Raman spectroelectrochemistry.

TOC GRAPHICS

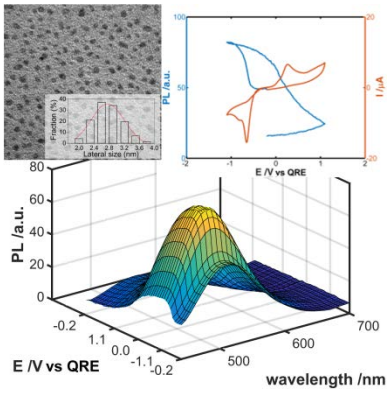

KEYWORDS Graphene quantum dots, electrochemistry, photoluminescence, spectroelectrochemistry.

Graphene quantum dots (GQD) represent a new member of the graphene family with unique and tunable electronic and optical properties arising from quantum confinement. Their size, crystallinity and composition-dependent properties make them very promising materials for applications in fields as diverse as energy conversion and storage,[1,2] catalysis,[3] synthesis,[4] sensing,[5] photovoltaics,[2,6] lighting[7], or biological applications.[8] It is expected that they can replace the well-known quantum dots based on metal chalcogenides as a result of their excellent

biocompatibility and solubility, low toxicity, high photostability against bleaching and blinking and low-cost preparation methods.[9]

In this context of broad multi-sectorial applicability, the optical properties of GQD are the subject of intense research.[8,10–24] GQD exhibit broad and tunable light absorption, a strong photoluminescence resulting from quantum confinement and high efficiency in up-conversion photoluminescence, properties that are largely dependent on GQD size and chemical composition.[16] Thus, substantial efforts are devoted to investigate the influence of the synthesis route and the resulting GQD features (size, number of layers, functional groups, defects, hybridization of the carbon network, etc.) on their optical properties with the aim of tailoring the material absorption, photoluminescence and photocatalytic properties according to the target application.[12,17,25] Photoluminescence is typically investigated in chemical equilibrium, comparing the experimental bands with theoretical studies for assignation of the bands to different electronic transitions.

In contrast, the electrochemical behavior of GQD has been comparatively less investigated. While the electrochemistry of graphene and related materials has been extensively explored[26], few reports have studied the redox properties of GQD. Indeed, most studies investigate the electrocatalytic activity of GQD-coated electrodes towards different model redox probes and electroactive analytes with a view of potential use for electroanalysis.[27,28] The intrinsic electrochemistry of GQD has been investigated in different works[29,30] in order to characterize this type of compounds. However, there are not electrochemical studies about the influence of the redox state of GQD on the optical properties of this new material. In this regard, spectroelectrochemistry is a valuable tool to study carbon nanomaterials and, thus, carbon nanotubes, graphene and carbon nanodots have been studied using spectroelectrochemistry.[31–37]

These techniques provide information about the dependence of the optical properties of these materials on the applied potential, the effect of electrochemical charge injection and removal to/from the nanomaterial and chemical transformations undergone by the nanostructures. Given the high photoluminescence (PL) of GQD, PL spectroelectrochemistry[38–40] in particular shall be especially suited to investigate how the redox state of GQD affect their optical properties. Indeed, PL dependence on the oxidation/reduction degree of GQD, graphene oxide quantum dots (GOQD) or reduced graphene oxide quantum dots (RGOQD) is still a current subject of debate due to controversial results.[11,15] While it seems that GQD multicolor emissions depend on the amount of oxygen, some studies showed that the emission of RGOQD does not match that of GOQD with comparable oxygen contents.[15] All studies on graphene derivatives so far differ in the oxidation/reduction method used, which comprise chemical methods,[25] high-temperature annealing[14,41] and/or photothermal methods.[10] However, to the best of our knowledge, there have not been attempts to tune the GQD redox state by electrochemical methods while simultaneously following changes in their optical properties. In this work, we have investigated PL changes induced by electrochemical charge injection and removal to/from GQD in order to shed more light on these complex processes, illustrating the potential of PL spectroelectrochemistry in the characterization and understanding of properties of this type of material. Moreover, electrochemistry allows more gradual and precise control of the reduction/oxidation degree, which combined with in-situ PL emission measurements provide direct information on the electronic and optical properties of GQD in each redox state.

GQD were synthesized by hydrothermal condensation of 1,3,6-trinitropyrene in a mixture of hydrazine hydrate and ammonia according to a protocol reported elsewhere.[42] Briefly, in a typical procedure pyrene (1 g) was nitrated into 1,3,6-trinitropyrene in 65% wt. HNO_3 (80 mL)

under refluxing and stirring for 16 h. After cooled to room temperature, the mixture was diluted with deionized (DI) water and filtered through a 0.22 μm nylon membrane. Part of the resultant 1,3,6-trinitropyrene (1 g) was dispersed by ultrasonication in a deionized water solution (0.1 L) containing 0.4 M ammonia and 1.5 M hydrazine hydrate for 1 h. The suspension was transferred to a Teflon-lined autoclave and heated at 200 ºC for 8 h. After cooled to room temperature, the GQD solution was filtered through a 0.22 μm nylon membrane to remove insoluble carbon product, and further dialysed in a dialysis bag (retained molecular weight: 3500 Da) for 1 day to remove salt and small molecules. The method yields highly crystalline GQD functionalized by OH and $NHNH_2$ moiety that exhibit a bright cyan fluorescence.

TEM and AFM images (Figure 1A and 1B) reveal that the GQD are very uniform in terms of lateral size and thickness, with an average size of 2.7 ± 0.4 nm and height of 1.5 ± 0.4 nm, indicating that most of the GQD were composed of 2-5 layers.

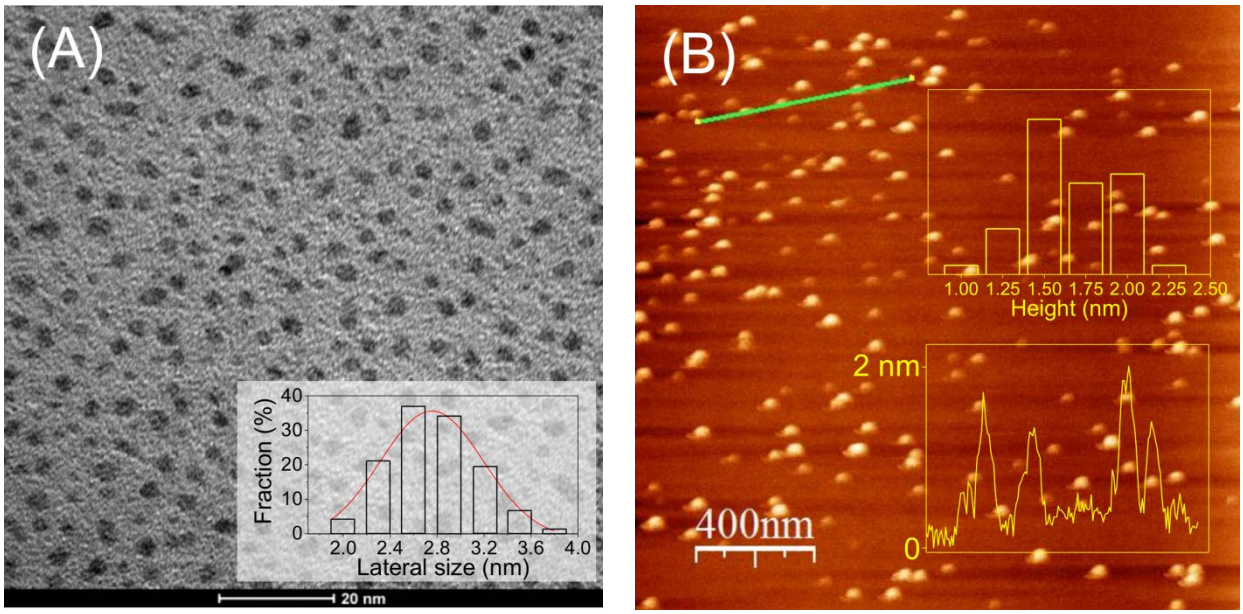

Figure 1. Microscopy characterization of GQD: (A) TEM image and corresponding lateral size distribution of GQD; (B) AFM image with height profile and corresponding thickness

distribution.

Raman spectroscopy at 633 nm (Figure S1A) shows the characteristic ordered G and disordered D bands of graphene-like materials at 1587 and 1372 cm^{-1}, respectively. The D to G band intensity ratio (I_D/I_G = 1.01) indicates the presence of a relative high proportion of defects and edge functional groups in the GQD as a result of their small lateral size.[1,12,43] Further Raman information was obtained at 532 nm (Figure S1B) where both D and G band were asymmetrically broadened revealing other overlapped vibrational modes.[44–48] The functional groups in the GQD were identified by FTIR spectroscopy. The main bands in the FTIR spectra (Figure S1C) can be assigned to the following vibrations: the C=C vibration at 1590 cm^{-1}, the N-H vibration from the $NHNH_2$ moiety at 3216 and 1618 cm^{-1}, the O-H vibration at 3360 cm^{-1} and the C-OH vibration at 1280 cm^{-1}. That is, the GQD have both amine and hydroxyl groups originated from the precursor and the media (hydrazine and ammonia) used in the condensation reaction.[42]

The presence of these functional groups was also corroborated by XPS analysis, as the high-resolution C 1s, O 1s and N 1s spectra revealed the signals from C-O (287.3 eV), C-N (401.2 eV), N-H (399.5 eV) and O-H (532.5 eV) bonds (Figure S2). The chemical composition of the GQD estimated from the XPS survey spectrum indicates 71.1 at.% C, 18.2 at.% O and 10.7 at.% N contents.

The optical properties of GQD were investigated by UV-visible absorption and fluorescence spectroscopy (Figure S3A and S3B). The UV-visible absorption spectrum (blue line in Figure S3A) exhibits three well-defined absorption bands located at 250, 290 and 400 nm, which can be assigned to the π-π^* transition of the aromatic sp^2 domains and electronic transitions between energy levels from the surface states arising from the functional groups.[1] In turn, the PL

excitation spectrum (black line in Figure S3A) features three intense bands at 260, 308 and 418 nm, in good agreement with the corresponding UV-vis absorption bands. The most intense PL emission, centered at 496 nm (red line in Figure S3A), is obtained with an excitation wavelength of 420 nm. However, the PL emission is excitation-dependent and when the excitation wavelength is increased from 340 to 460 nm the PL emission peak slightly shifts to longer wavelengths (from 475 to 505 nm) and at long excitation wavelengths the PL intensity decreases sharply (Figure S3B). This excitation-dependent PL emission has been commonly observed in GQD and has been ascribed to excitation of different sized GQD or conjugated sp^2 domains in the GQD carbon network.

Charge injection/removal to/from GQD was carried out by cyclic voltammetry (Figure S4) at different scan rates from 0.01 to 0.05 V s^{-1} in a GQD solution (0.00145 mg L^{-1}) in 0.1 M $LiClO_4$. The potential was scanned from -0.20 V to -1.10 V and back to +1.10 V, finishing at -0.20 V. In this potential range GQD were reduced and oxidized, undergoing two irreversible reduction processes at -0.61 and -0.75 V during the cathodic scan and one irreversible oxidation process at +0.46 V during the anodic scan (potential values obtained at the lowest scan rate). The reduction process is dependent on the scan rate indicating an adsorption process and the oxidation peak is dependent on the square root of the scan rate indicating a process controlled by diffusion. It is noteworthy that a small oxidation prewave is observed around +0.10 V. The electrochemical behavior is quite complex and although these voltammetric peaks are related to reduction and oxidation of the GQD, a detailed interpretation of the cyclic voltammogram (CV) is not straightforward from the electrochemical data alone. In order to understand the electron transfer processes taking place at the GQD solution/electrode interface and to assess how these processes affect the GQD luminescence, PL spectroelectrochemistry was used. A 385 nm LED light source

was selected to perform PL spectroelectrochemistry measurements using a near-normal configuration, as described in the Supporting Information. This experimental setup enables following not only the GQD PL but also absorbance changes at the LED wavelength during cyclic voltammetry.

Figure 2A shows CV and voltabsorptogram (VA) at 385 nm recorded during the potential scan in a 0.00145 mg L^{-1} GQD solution in 0.1 M $LiClO_4$, using an integration time of 200 ms. As can be seen, an increase in absorbance at 385 nm from -0.75 V downwards occurs during the cathodic sweep concomitantly with the two reduction peaks observed in the CV.

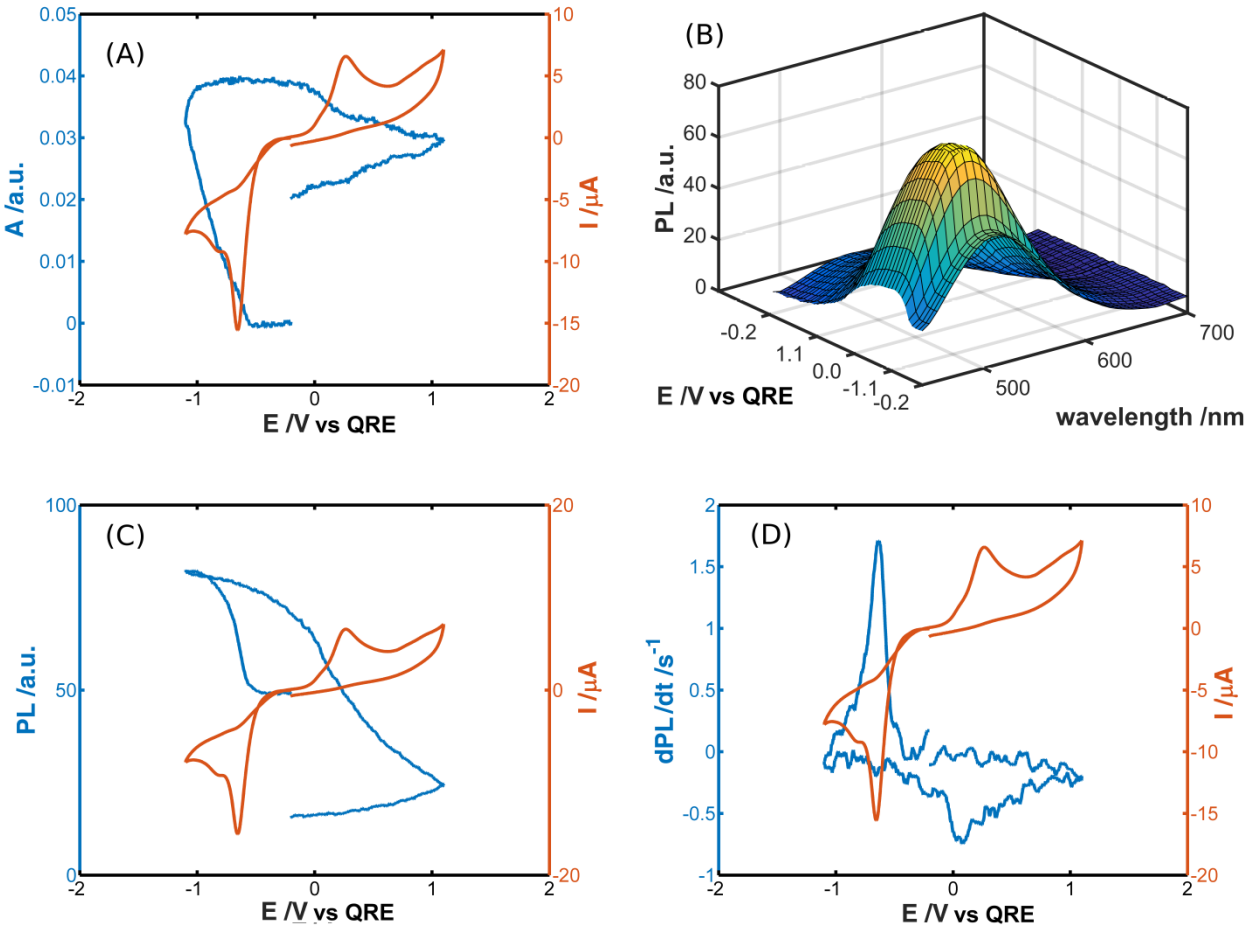

Figure 2. (A) CV (brown line) and voltabsorptogram at 385 nm (blue line); (B) Evolution of the PL emission spectra obtained during the cyclic voltammetry**;** (C) CV (brown line) and PL at 500

nm (blue line); and (D) CV (brown line) and derivative of PL intensity at 500 nm (blue line) recorded during the potential scan carried out in a 0.00145 mg L^{-1} GQD solution in 0.1 M $LiClO_4$. $E_i = E_f$ = -0.20 V, E_{v1}=-1.10 V, E_{v2} = +1.10 V, v = 0.010 V s^{-1}, integration time = 200 ms.

Spectroelectrochemistry was also carried out in a solution containing only the supporting electrolyte (0.1 M $LiClO_4$), Figure S5. In this case, Figure S5A, only the second reduction peak is observed as well as a very small change in absorbance, Figure S5B, indicating the reduction of defects on the carbon screen printed electrode. In the anodic scan, Figure 2A, absorbance at 385 nm remains almost constant in the cathodic region (between -1.00 and 0.00 V) but starts decreasing at the oxidation prewave potential and continues decreasing simultaneously with the oxidation peak at +0.46 V up to the end of the scan in the anodic region. This peak is not observed in the blank experiment, Figure S5A, with the change of absorbance being also negligible, Figure S5B.

The absorption of radiation at 385 nm has an associated PL emission band with a maximum at ca. 500 nm, Figure S3B. Figure 2B shows the evolution of the PL emission spectra during the voltammetric scan plotted against potential to follow better PL evolution. The PL band centered at 500 nm increases during the cathodic scan and this trend is reversed in the anodic scan, with PL decreasing drastically in the anodic region.

A more detailed picture of PL changes with GQD redox state can be drawn from Figure 2C, where the CV and the evolution of PL emission intensity at 500 nm with the potential are plotted together. Figure 2C corroborates once more that the potential changes of PL emission intensity at 500 nm are related to the redox processes in the CV. Thus, the first reduction peak at -0.46 V is accompanied by an increase of PL emission intensity. This PL enhancement can be rationalized

in terms of reduction of defects in GQD, yielding a relative higher content of sp^2 domains. It is noteworthy that PL changes are negligible during the second reduction process at -0.75 V, and the change in PL is attributed to the first reduction peak, as it will be inferred from the derivative PL shown below. Therefore, this second reduction process cannot be related to changes in the energy levels of the GQD associated with PL emission. PL emission intensity decreases slowly from the start of anodic scan and more abruptly at +0.10 V, potential of the anodic peak prewave where there was also a pronounced absorbance drop. Hence quenching of both optical responses are associated with the oxidation of GQD. PL intensity continues decreasing until the end of the scan in the anodic region revealing the irreversible oxidation of GQD. This agreement between the CV peaks and PL intensity changes is more clearly observed plotting the derivative of the PL intensity at 500 nm (dPL/dt) against potential, Figure 2D. The first cathodic peak in the CV matches the position of the maximum value of dPL/dt, while the minimum of the derivative of PL intensity corresponds to the oxidation peak prewave.

Therefore, PL spectroelectrochemistry reveals that GQD PL intensity is enhanced upon reduction and the process is electrochemically quasi-reversible, recovering the initial conditions during the anodic scan in the cathodic potential region. However, when the anodic potential is further increased, GQD are oxidized and PL intensity decreases below the initial value due to the irreversible oxidation of GQD.

The spectroelectrochemical trends at one wavelength provide temporal information about GQD PL intensity dependence on their redox state, but more insight about the origin of emission enhancement/quenching can be gained analyzing the evolution of the PL emission spectra at all wavelengths with potential. Figure 3A shows PL emission spectra at different potentials during the cathodic sweep. As can be seen, the PL band increase is not symmetrical, resulting in a small

blue shifting from 507 to 497 nm. This shift is better resolved by plotting the variation of PL intensity (ΔPL) at each potential with respect to the initial PL emission spectrum at -0.20 V, a potential where GQD are stable, Figure 3B.

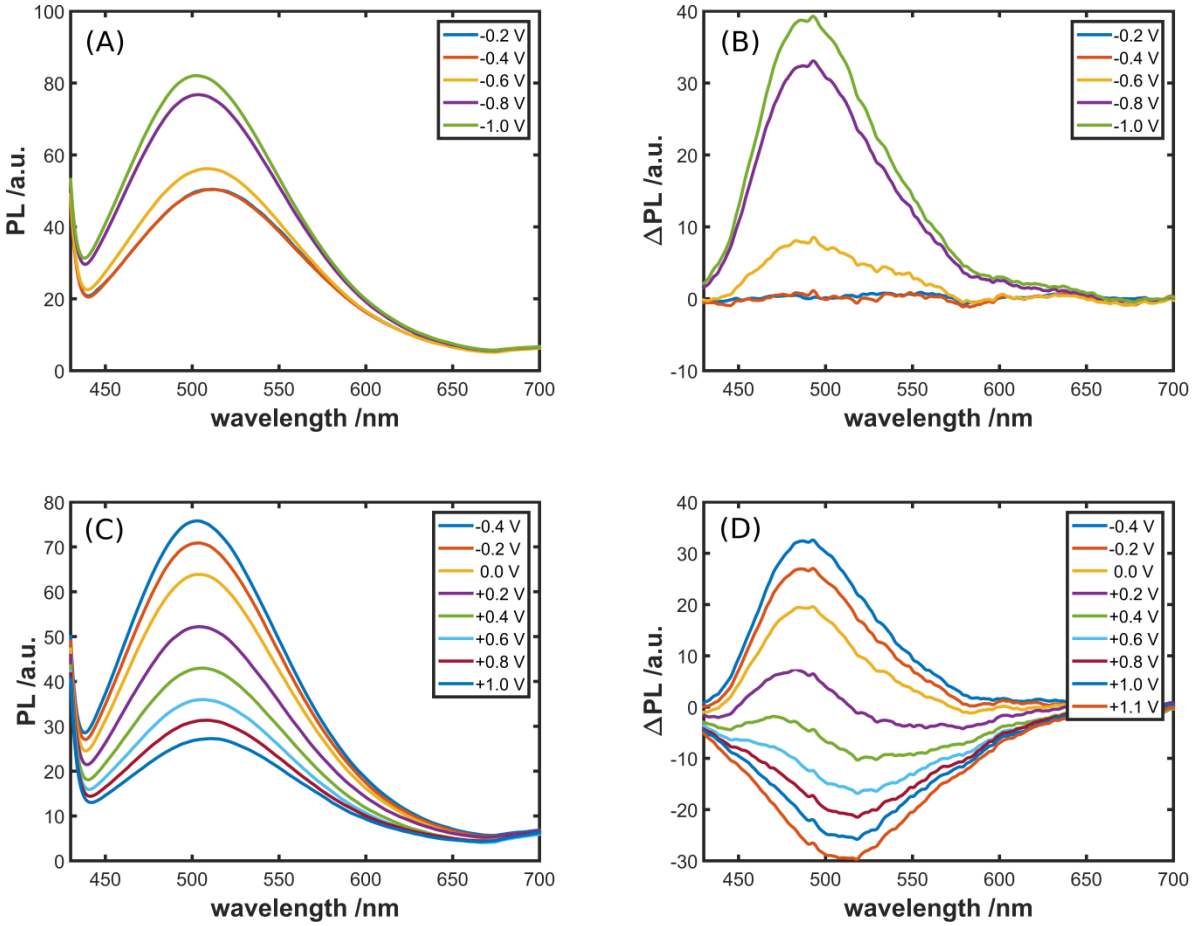

Figure 3. (A) PL emission spectra during the cathodic scan; (B) PL intensity change with respect to the initial emission spectrum at -0.20 V during the cathodic scan: (C) PL emission spectra during the anodic scan; and (D) PL intensity change with respect to the initial emission spectrum at -0.20 V during the anodic scan. All signals obtained at different potentials in a 0.00145 mg L^{-1} GQD solution in 0.1 M $LiClO_4$. E_i=E_f = -0.20 V, E_{v1} = -1.10 V, E_{v2} = +1.10 V, v = 0.010 V s^{-1}, integration time = 200 ms.

The growth of a ΔPL band at shorter wavelengths (487 nm) than that of unbiased GQD (507 nm) is clearly observed, evidencing the blue shift of the PL emission spectrum upon charge injection to GQD. In fact, the new band appearing during the reduction process peaks at 487 nm. From the difference spectra, ΔPL, the PL emission band can be deconvoluted into two different bands corresponding to diverse electronic transitions in the GQD.[12] The band at longer wavelengths, around 507 nm, can be attributed to the $n \rightarrow \pi^*$ electronic transition between energy levels arising from the functional groups and the band at shorter wavelengths, around 487 nm, can be assigned to the $\pi \rightarrow \pi^*$ transition of the aromatic sp^2 domains in the GQD network.

A similar analysis of the evolution of the PL emission spectra can be performed for the anodic scan, Figure 3C and Figure 3D. Here, the PL band intensity decreases and red shifts with the anodic potential and again the potential dependence of PL is better resolved by plotting PL intensity changes with potential taking the PL emission spectrum at -0.20 V as reference (Figure 3D). Red shifting of the ΔPL band largely depends on the applied potential, revealing the quenching of different electronic transitions between energy levels in GQD at different oxidation degree. As can be seen, at the onset of the anodic scan (from -0.4 V to 0.00 V) the ΔPL band centered at 487 nm, related to the $\pi \rightarrow \pi^*$ transition in the aromatic sp^2 domains[12] starts to bleach first. At higher anodic potentials (from +0.20 V upwards), bleaching of the ΔPL band at longer wavelengths (peaking at 507 nm) occurs, which is related to the $n \rightarrow \pi^*$ transition between energy levels from the functional groups.[12]

As was stated above a control PL spectroelectrochemistry experiment was also performed in a solution containing only the supporting electrolyte (0.1 M $LiClO_4$), Figure S5. In this case, a

single reduction peak around -0.85 V and the oxidation of the carbon screen printed electrode were observed without changes of PL emission, Figure S5C, confirming that the potential dependent PL intensity changes in GQD solutions are only related to electronic transitions in GQD. The cathodic peak in $LiClO_4$ 0.1 M (Figure S5A) can be assigned to the reduction of oxygen and functional groups in the screen printed carbon electrode not inducing PL emission (Figure S5C). Likewise, other carbon allotropes like carbon nanotubes or graphene did not yield measurable PL emission under comparable experimental conditions. It has to be noted that when a blank experiment (in a GQD-free solution) was performed with a SPE previously used to reduce GQD, a small change of PL emission was observed, confirming GQD adsorption during the cathodic scan.

Therefore, taking into account the spectroelectrochemical experiments in GQD solutions and bare electrolyte, it can be concluded that PL intensity increases during GQD reduction as a result of a migration of excitons from the sp^3 defect states to the sp^2 domains that are responsible of the GQD blue PL emission.[15] Raman spectroelectrochemistry experiments were performed in a 0.00145 mg L^{-1} GQD solution in 0.1 M $LiClO_4$, applying different cathodic potentials to show the relationship between the charge injection and the change in the vibrational spectrum of the GQD. A blank experiment was also performed in GQD-free 0.1 M $LiClO_4$ solution. In this blank experiment, only the Raman bands ascribed to the carbon paste of the SPE were observed (1357 cm^{-1} and 1600 cm^{-1}, Figure S6) and were unaffected by the potential. It is noteworthy that GQD Raman spectra in solution at 532 nm (Figure S6) show the same vibrational bands as in the solid samplebut with different intensity as a result of different interactions between GQD in powder samples and dissolved. As can be observed in the evolution of the Raman spectra (Figure S6), the intensity of the Raman bands decreased during the reduction of the GQD. These are

preliminary results that confirm a change in the GQD structure during reduction, but more experiments should be done to elucidate the exact nature of functional groups involved. The PL emission blue shift occurring during reduction points at larger size/number of sp^2 carbon domains associated to $\pi \rightarrow \pi^*$ transitions. Similar blue shifting upon reduction was also observed for carbon nanodots[37]. This electrochemical process is quasi-reversible because the oxidation prewave around +0.10 V is clearly related to depletion of $\pi \rightarrow \pi^*$ transitions (Figures 2C, 3C and 3D) and PL intensity recovered the initial value when the voltammetric scan was stopped at +0.20 V. However, when the anodic potential was higher, irreversible GQD oxidation occurs, leading to PL bleaching. With increasing GQD oxidation level, the density and size of sp^2 carbon domains is lowered and the content of oxygen-bonded sp^3 carbon increased, causing the disappearance of blue emission from sp^2 nanodomains and the red shift of the PL emission associated with the prevalent $n \rightarrow \pi^*$ transition. It should be pointed out that irreversible GQD oxidation and concomitant PL emission bleaching also take place when the potential was scanned initially in the anodic direction (Figure S7).

Overall, the evolution of PL emission bands during the electrochemical oxidation and reduction agrees with the behavior described in literature for GOQD and RGOQD where the oxidation degree was tuned varying the ratio of oxidizing and reducing agents.[15] However, in their case irreversible PL emission changes were noted for GOQD and RGOQD with similar oxygen content. Here performing simultaneously charge injection and in-situ PL measurement allowed us to identify the potential range and associated redox states where reversible PL emission changes occur. Moreover, a relationship between the PL quantum yield (QY) value and the electrical charge injected from/to the GQD was obtained. A QY of 0.44 was first determined for the GQD using 9,10-diphenylanthracene as standard. This value was used to obtain the ratio

of emitted-to-absorbed photons in the PL spectroelectrochemistry experiments. A maximum QY of 0.55 was obtained at -0.80 V during the reduction process. On the contrary, a minimum QY of 0.12 was obtained at the end of the CV because most of the GQD were oxidized. An almost linear relationship between injected charge and QY was observed during the reduction process, from -0.40 V to -0.80 V, (Figure S8) reaching a plateau around -0.80 V where the first reduction of the GQD has taken place. Therefore, this experimental setup allowed us to calculate the QY for different redox states, providing information on the evolution of the QY with the injected charge.

The PL and electrochemical behavior of GQD differs from that observed by Strauss et al. for carbon nanodots,[37] illustrating the complex electrochemistry of these carbon nanostructures. Strauss et al. indicate that the fluorescence of CND is trap mediated, which could also explain PL changes in GQDs. In this scenario, when the fermi level of the electrode increases (cathodic scan) the trap states could be filled, enabling photoexcited electrons to relax from density of states at higher energy level, yielding a blue shifting. In turn, depopulating the states by scanning the potential in the anodic direction would dischar these states, yielding a decrease in PL. This interpretation is compatible with a migration of excitons within the sp^2 clusters towards the sp^3 defect states. That is, additional studies of this family of highly luminescent carbon nanostructures would be required to fully understand the PL dependence on the injected charge and the exact nature of the PL emission processes.

In conclusion, we have shown that the multiple-nature information obtained by combined absorption and PL emission spectroelectrochemistry has proven very useful to characterize luminescent GQD upon charge injection. PL emission spectroelectrochemistry yields direct in-situ evidence of the redox state dependence of GQD luminescence, enabling us to identify the

associated electronic transitions responsible for the enhanced/bleached emission. Moreover, in contrast with ex-situ chemical tuning of GQD redox state and subsequent probing of GQD PL, following in-situ PL change upon electrochemical charge injection makes it possible to tune reversibly PL emission in GQD.

After this pioneer work illustrating the power of PL spectroelectrochemistry to investigate GQD, further experiments will be done to study GQD with different chemical composition, band gaps and emissive properties and their behavior under different charge conditions that can be easily controlled by electrochemistry.

ASSOCIATED CONTENT

Supporting Information

The Supporting Information is available free of charge on the ACS Publications website. Experimental section (Materials, Instrumentation). Figure S1, Raman an FTIR analysis of the GQD. Figure S2, XPS analysis of the GQD. Figure S3, UV-visible absorption, PL excitation and emission spectra of GQD. Figure S4, Cyclic voltammograms at different scan rates. Figure S5, PL spectroelectrochemistry in a blank solution. Figure S6, Raman Spectroelectrochemistry of the GQD during the reduction process. Figure S7, PL spectroelectrochemistry of the GQD starting in anodic direction. Figure S8, Evolution of the QY with the electrical charge.

ACKNOWLEDGMENTS

Support from Ministerio de Economía y Competitividad (CTQ2014-55583-R, CTQ2014-61914-EXP, CTQ2015-71955-REDT), Junta de Castilla y León (BU033-U16) and Basque Government under the ELKARTEK Program (ACTIMAT project, grant number KK-2015/00094 and KK-2016/00097) is gratefully acknowledged. D.I. thanks Ministerio de Economía y Competitividad for his post-doctoral fellowship (CTQ2014-61914-EXP).

REFERENCES

(1) Zhang, Z.; Zhang, J.; Chen, N.; Qu, L.; Kroto, H. W.; Heath, J. R.; O'Brien, S. C.; Curl, R. F.; Smalley, R. E.; Iijima, S.; et al. Graphene Quantum Dots: An Emerging Material for Energy-Related Applications and beyond. *Energy Environ. Sci.* **2012**, *5* (10), 8869.

(2) Li, X.; Rui, M.; Song, J.; Shen, Z.; Zeng, H. Carbon and Graphene Quantum Dots for Optoelectronic and Energy Devices: A Review. *Adv. Funct. Mater.* **2015**, *25* (31), 4929–4947.

(3) Fernando, K. A. S.; Sahu, S.; Liu, Y.; Lewis, W. K.; Guliants, E. A.; Jafariyan, A.; Wang, P.; Bunker, C. E.; Sun, Y. P. Carbon Quantum Dots and Applications in Photocatalytic Energy Conversion. *ACS Appl. Mater. Interfaces* **2015**, *7* (16), 8363–8376.

(4) Liu, Y.; Xu, M.; Zhu, X.; Xie, M.; Su, Y.; Hu, N.; Yang, Z.; Zhang, Y. Synthesis of Carbon Nanotubes on Graphene Quantum Dot Surface by Catalyst Free Chemical Vapor Deposition. *Carbon* **2014**, *68*, 399–405.

(5) Benítez-Martínez, S.; Valcárcel, M. Graphene Quantum Dots in Analytical Science. *TrAC Trends Anal. Chem.* **2015**, *72*, 93–113.

(6) Guo, C. X.; Yang, H. Bin; Sheng, Z. M.; Lu, Z. S.; Song, Q. L.; Li, C. M. Layered Graphene/Quantum Dots for Photovoltaic Devices. *Angew. Chemie Int. Ed.* **2010**, *49* (17), 3014–3017.

(7) Baker, S. N.; Baker, G. A. Luminescent Carbon Nanodots: Emergent Nanolights. *Angew. Chemie Int. Ed.* **2010**, *49* (38), 6726–6744.

(8) Zheng, X. T.; Ananthanarayanan, A.; Luo, K. Q.; Chen, P. Glowing Graphene Quantum Dots and Carbon Dots: Properties, Syntheses, and Biological Applications. *Small* **2015**, *11* (14), 1620–1636.

(9) Bacon, M.; Bradley, S. J.; Nann, T. Graphene Quantum Dots. *Part. Part. Syst. Charact.* **2014**, *31* (4), 415–428.

(10) Eda, G.; Lin, Y. Y.; Mattevi, C.; Yamaguchi, H.; Chen, H. A.; Chen, I. S.; Chen, C. W.; Chhowalla, M. Blue Photoluminescence from Chemically Derived Graphene Oxide. *Adv. Mater.* **2010**, *22* (4), 505–509.

(11) Li, Y.; Liu, X.; Wang, J.; Liu, H.; Li, S.; Hou, Y.; Wan, W.; Xue, W.-D.; Ma, N.; Zhang, J. Z. Chemical Nature of Redox-Controlled Photoluminescence of Graphene Quantum Dots by Post-Synthesis Treatment. *J. Phys. Chem. C* **2016**, 120 (45), pp 26004–26011.

(12) Yeh, T.-F.; Huang, W.-L.; Chung, C.-J.; Chiang, I.-T.; Chen, L.-C.; Chang, H.-Y.; Su, W.-C.; Cheng, C.; Chen, S.-J.; Teng, H. Elucidating Quantum Confinement in Graphene Oxide Dots Based On Excitation-Wavelength-Independent Photoluminescence. *J. Phys. Chem. Lett.* **2016**, *7* (11), 2087–2092.

(13) Li, M.; Cushing, S. K.; Zhou, X.; Guo, S.; Wu, N. Fingerprinting Photoluminescence of Functional Groups in Graphene Oxide. *J. Mater. Chem.* **2012**, *22* (44), 23374–23379.

(14) Loh, K. P.; Bao, Q.; Eda, G.; Chhowalla, M. Graphene Oxide as a Chemically Tunable Platform for Optical Applications. *Nat. Chem.* **2010**, *2* (12), 1015–1024.

(15) Jang, M.-H.; Ha, H. D.; Lee, E.-S.; Liu, F.; Kim, Y.-H.; Seo, T. S.; Cho, Y.-H. Is the Chain of Oxidation and Reduction Process Reversible in Luminescent Graphene Quantum Dots? *Small* **2015**, *11* (31), 3773–3781.

(16) Sk, M. A.; Ananthanarayanan, A.; Huang, L.; Lim, K. H.; Chen, P. Revealing the Tunable Photoluminescence Properties of Graphene Quantum Dots. *J. Mater. Chem. C* **2014**, *2* (34), 6954-6960.

(17) Das, S. K.; Luk, C. M.; Martin, W. E.; Tang, L.; Kim, D. Y.; Lau, S. P.; Richards, C. I. Size and Dopant Dependent Single Particle Fluorescence Properties of Graphene Quantum Dots. *J. Phys. Chem. C* **2015**, *119* (31), 17988–17994.

(18) Zhu, S.; Song, Y.; Zhao, X.; Shao, J.; Zhang, J.; Yang, B. The Photoluminescence Mechanism in Carbon Dots (Graphene Quantum Dots, Carbon Nanodots, and Polymer Dots): Current State and Future Perspective. *Nano Res.* **2015**, *8* (2), 355–381.

(19) Chien, C. T.; Li, S. S.; Lai, W. J.; Yeh, Y. C.; Chen, H. A.; Chen, I. S.; Chen, L. C.; Chen, K. H.; Nemoto, T.; Isoda, S.; et al. Tunable Photoluminescence from Graphene Oxide. *Angew. Chemie - Int. Ed.* **2012**, *51* (27), 6662–6666.

(20) Jin, S. H.; Jun, G. H.; Hong, S. H.; Jeon, S.; Science, M.; Technology, I. Tuning the Photoluminescence of Graphene Quantum Dots through the Charge Transfer Effect of Functional Groups. ACS Nano **2013**, 1239–1245.

(21) Hassanien, A. S.; Shedeed, R. A.; Allam, N. K. Graphene Quantum Sheets with Multiband Emission: Unravelling the Molecular Origin of Graphene Quantum Dots. *J. Phys. Chem. C* **2016**, 120, 21678-21864.

(22) Zhu, S.; Wang, L.; Li, B.; Song, Y.; Zhao, X.; Zhang, G.; Zhang, S.; Lu, S.; Zhang, J.; Wang, H.; et al. Investigation of Photoluminescence Mechanism of Graphene Quantum Dots and Evaluation of Their Assembly into Polymer Dots. *Carbon* **2014**, *77*, 462–472.

(23) Tetsuka, H.; Asahi, R.; Nagoya, A.; Okamoto, K.; Tajima, I.; Ohta, R.; Okamoto, A. Optically Tunable Amino-Functionalized Graphene Quantum Dots. *Adv. Mater.* **2012**, *24* (39), 5333–5338.

(24) Yang, F.; LeCroy, G. E.; Wang, P.; Liang, W.; Chen, J.; Fernando, K. A. S.; Bunker, C. E.; Qian, H.; Sun, Y.-P. Functionalization of Carbon Nanoparticles and Defunctionalization—Toward Structural and Mechanistic Elucidation of Carbon "Quantum" Dots. *J. Phys. Chem. C* **2016**, *120* (44), 25604–25611.

(25) Zhu, S.; Zhang, J.; Tang, S.; Qiao, C.; Wang, L.; Wang, H.; Liu, X.; Li, B.; Li, Y.; Yu, W.; et al. Surface Chemistry Routes to Modulate the Photoluminescence of Graphene Quantum Dots: From Fluorescence Mechanism to Up-Conversion Bioimaging Applications. *Adv. Funct. Mater.* **2012**, *22* (22), 4732–4740.

(26) Ambrosi, A.; Chua, C. K.; Bonanni, A.; Pumera, M. Electrochemistry of Graphene and Related Materials. *Chem. Rev.* **2014**, *114* (14), 7150–7188.

(27) Lim, C. S.; Hola, K.; Ambrosi, A.; Zboril, R.; Pumera, M. Graphene and Carbon Quantum Dots Electrochemistry. *Electrochem. Commun.* **2015**, *52*, 75–79.

(28) Zhang, Y.; Wu, C.; Zhou, X.; Wu, X.; Yang, Y.; Wu, H.; Guo, S.; Zhang, J. Graphene Quantum Dots/gold Electrode and Its Application in Living Cell H2O2 Detection. *Nanoscale* **2013**, *5* (5), 1816-1819.

(29) Shinde, D. B.; Pillai, V. K. Electrochemical Resolution of Multiple Redox Events for Graphene Quantum Dots. *Angew. Chemie - Int. Ed.* **2013**, *52* (9), 2482–2485.

(30) Skaltsas, T.; Stergiou, A.; Chronopoulos, D. D.; Zhao, S.; Shinohara, H.; Tagmatarchis, N. All-Carbon Nanosized Hybrid Materials: Fluorescent Carbon Dots Conjugated to Multiwalled Carbon Nanotubes. *J. Phys. Chem. C* **2016**, *120* (16), 8550–8558.

(31) Ibañez, D.; Garoz-Ruiz, J.; Heras, A.; Colina, A. Simultaneous UV–Visible Absorption and Raman Spectroelectrochemistry. *Anal. Chem.* **2016**, *88* (16), 8210–8217.

(32) Hernández, C. N.; García, M. B. G.; Santos, D. H.; Heras, M. A.; Colina, A.; Fanjul-Bolado, P. Aqueous UV-VIS Spectroelectrochemical Study of the Voltammetric Reduction of Graphene Oxide on Screen-Printed Carbon Electrodes. *Electrochem. Commun.* **2016**, *64*, 65–68.

(33) Garoz-Ruiz, J.; Ibañez, D.; Romero, E. C.; Ruiz, V.; Heras, A.; Colina, A. Optically Transparent Electrodes for Spectroelectrochemistry Fabricated with Graphene Nanoplatelets and Single-Walled Carbon Nanotubes. *RSC Adv.* **2016**, *6* (37), 31431–31439.

(34) Kavan, L.; Dunsch, L. Spectroelectrochemistry of Carbon Nanostructures. *Chemphyschem* **2007**, *8* (7), 974–998.

(35) Ibañez, D.; Romero, E. C.; Heras, A.; Colina, A. Dynamic Raman Spectroelectrochemistry of Single Walled Carbon Nanotubes Modified Electrodes Using a Langmuir-Schaefer Method. *Electrochim. Acta* **2014**, *129*, 171–176.

(36) Colina, A.; Ruiz, V.; Heras, A.; Ochoteco, E.; Kauppinen, E.; López-Palacios, J. Low Resolution Raman Spectroelectrochemistry of Single Walled Carbon Nanotube Electrodes. *Electrochim. Acta* **2011**, *56* (3), 1294–1299.

(37) Strauss, V.; Kahnt, A.; Zolnhofer, E. M.; Meyer, K.; Maid, H.; Placht, C.; Bauer, W.; Nacken, T. J.; Peukert, W.; Etschel, S. H.; Halik, M.; Guldi, D. M.. Assigning Electronic States in Carbon Nanodots. *Adv. Funct. Mater.* **2016**, *26* (44), 7975–7985.

(38) Galland, C.; Ghosh, Y.; Steinbrück, A.; Sykora, M.; Hollingsworth, J. A; Klimov, V. I.; Htoon, H. Two Types of Luminescence Blinking Revealed by Spectroelectrochemistry of Single Quantum Dots. *Nature* **2011**, *479* (7372), 203–207.

(39) Weaver, A. L.; Gamelin, D. R. Photoluminescence Brightening via Electrochemical Trap Passivation in ZnSe and Mn^{2+}-Doped ZnSe Quantum Dots. *J. Am. Chem. Soc.* **2012**, *134* (15), 6819–6825.

(40) Nagatani, H.; Fermín, D. J.; Girault, H. H. A Kinetic Model for Adsorption and Transfer of Ionic Species at Polarized Liquid|liquid Interfaces as Studied by Potential Modulated Fluorescence Spectroscopy. *J. Phys. Chem. B* **2001**, *105* (39), 9463–9473.

(41) Khai, T. Van; Na, H. G.; Kwak, D. S.; Kwon, Y. J.; Ham, H.; Shim, K. B. H.; Kim, H. W. Significant Enhancement in Blue Emission and Electrical Conductivity of N-Doped Graphene. *J. Mater. Chem.* **2012**, *22* (34), 1166–1169.

(42) Wang, L.; Wang, Y.; Xu, T.; Liao, H.; Yao, C.; Liu, Y.; Li, Z.; Chen, Z.; Pan, D.; Sun, L.; Wu, M. Gram-Scale Synthesis of Single-Crystalline Graphene Quantum Dots with Superior Optical Properties. *Nat. Commun.* **2014**, *5*, 5357.

(43) Pan, D.; Guo, L.; Zhang, J.; Xi, C.; Xue, Q.; Huang, H.; Li, J.; Zhang, Z.; Yu, W.; Chen, Z.; Li, Z; Wu, M. Cutting sp^2 Clusters in Graphene Sheets into Colloidal Graphene Quantum Dots with Strong Green Fluorescence. *J. Mater. Chem.* **2012**, *22* (8), 3314-3318.

(44) Hassanien, A. S.; Shedeed, R. A.; Allam, N. K. Graphene Quantum Sheets with Multiband Emission: Unravelling the Molecular Origin of Graphene Quantum Dots. *J. Phys. Chem. C* **2016**, *120* (38), 21678–21684.

(45) Negri, F.; Castiglioni, C.; Tommasini, M.; Zerbi, G. A Computational Study of the Raman Spectra of Large Polycyclic Aromatic Hydrocarbons: Toward Molecularly Defined Subunits of Graphite. *J. Phys. Chem. A* **2002**, *106* (14), 3306–3317.

(46) Cançado, L. G.; Pimenta, M. A.; Neves, B. R. A.; Dantas, M. S. S.; Jorio, A. Influence of the Atomic Structure on the Raman Spectra of Graphite Edges. *Phys. Rev. Lett.* **2004**, *93* (24), 247401.

(47) Kudin, K. N.; Ozbas, B.; Schniepp, H. C.; Prud'homme, R. K.; Aksay, I. A.; Car, R. Raman Spectra of Graphite Oxide and Functionalized Graphene Sheets. *Nano Lett.* **2008**, *8* (1), 36–41.

(48) Song, Y.; Chen, S. Graphene Quantum-Dot-Supported Platinum Nanoparticles: Defect-Mediated Electrocatalytic Activity in Oxygen Reduction. *ACS Appl. Mater. Interfaces* **2014**, *6* (16), 14050–14060.